Chinese Journal of Natural Medicines

Esculetin triggers ferroptosis *via* inhibition of the Nrf2–xCT/GPx4 axis in hepatocellular carcinoma

Zhixin Qu, Jing Zeng, Laifeng Zeng, Xianmei Li, Fenghua Zhang

Citation: Zhixin Qu, Jing Zeng, Laifeng Zeng, Xianmei Li, Fenghua Zhang, Esculetin triggers ferroptosis *via* inhibition of the Nrf2–xCT/GPx4 axis in hepatocellular carcinoma, Chinese Journal of Natural Medicines, 2025, 23(4), 443–456. doi: 10.1016/S1875–5364(25)60853–3.

View online: https://doi.org/10.1016/S1875–5364(25)60853–3

Chinese Journal of Natural Medicines 23 (2025) 443-456

Contents lists available at ScienceDirect

Chinese Journal of Natural Medicines

journal homepage: www.cjnmcpu.com/

Original article

Esculetin triggers ferroptosis *via* inhibition of the Nrf2-xCT/GPx4 axis in hepatocellular carcinoma

Zhixin Qu[a], Jing Zeng[a], Laifeng Zeng[b], Xianmei Li[b,*], Fenghua Zhang[a,*]

[a] *Key Laboratory of Gastrointestinal Cancer (Ministry of Education), School of Basic Medical Sciences, Fujian Medical University, Fuzhou 350122, China*
[b] *Fujian Key Laboratory of Integrative Medicine on Geriatrics, Academy of Integrative Medicine, Fujian University of Traditional Chinese Medicine, Fuzhou 350122, China*

ARTICLE INFO

Article history:
Received 5 January 2024
Revised 27 April 2024
Accepted 4 May 2024
Available online 20 April 2025

Keywords:
Esculetin
Ferroptosis
Hepatocellular carcinoma
Nrf2-xCT/GPx4 axis
Zebrafish

ABSTRACT

Esculetin, a natural dihydroxy coumarin derived from the Chinese herbal medicine *Cortex Fraxini*, has demonstrated significant pharmacological activities, including anticancer properties. Ferroptosis, an iron-dependent form of regulated cell death, has garnered considerable attention due to its lethal effect on tumor cells. However, the exact role of ferroptosis in esculetin-mediated anti-hepatocellular carcinoma (HCC) effects remains poorly understood. This study investigated the impact of esculetin on HCC cells both *in vitro* and *in vivo*. The findings indicate that esculetin effectively inhibited the growth of HCC cells. Importantly, esculetin promoted the accumulation of intracellular Fe^{2+}, leading to an increase in ROS production through the Fenton reaction. This event subsequently induced lipid peroxidation (LPO) and triggered ferroptosis within the HCC cells. The occurrence of ferroptosis was confirmed by the elevation of malondialdehyde (MDA) levels, the depletion of glutathione peroxidase (GSH-Px) activity, and the disruption of mitochondrial morphology. Notably, the inhibitor of ferroptosis, ferrostatin-1 (Fer-1), attenuated the anti-tumor effect of esculetin in HCC cells. Furthermore, the findings revealed that esculetin inhibited the Nrf2-xCT/GPx4 axis signaling in HCC cells. Overexpression of Nrf2 upregulated the expression of downstream SLC7A11 and GPX4, consequently alleviating esculetin-induced ferroptosis. In conclusion, this study suggests that esculetin exerts an anti-HCC effect by inhibiting the activity of the Nrf2-xCT/GPx4 axis, thereby triggering ferroptosis in HCC cells. These findings may contribute to the potential clinical use of esculetin as a candidate for HCC treatment.

1. Introduction

Liver cancer is the sixth most commonly diagnosed cancer worldwide and the third leading cause of cancer-related deaths [1]. Hepatocellular carcinoma (HCC) accounts for approximately 90% of primary liver cancers [2], posing significant challenges due to its high morbidity and mortality rates. While surgical intervention is an effective treatment option for early-stage HCC, it is often not applicable to patients in advanced stages. As a result, many HCC patients rely on chemical drugs, such as Sorafenib and Renvatinib, to extend their survival time. However, these drugs frequently come with notable side effects and may not be effective for all patients [3]. Consequently, there is an urgent need to discover novel, effective drugs for the treatment of HCC.

Esculetin, an active component of the Chinese herbal medicine *Cortex Fraxini*, has been reported to possess various biological activities, including anti-inflammatory [4], antiviral [5], antioxidant [6], and anti-tumor [7] properties. Regarding its anticancer effects, esculetin has been found to induce apoptosis in different cancer types, including HCC. For example, in the HCC cell line SMMC-7721, esculetin has been shown to increase the activity of caspase-3 and caspase-9, reduce mitochondrial membrane potential, increase the expression of Bax, and decrease the expression of Bcl-2, thereby demonstrating its potential anti-HCC effects through the initiation of a mitochondrial-dependent apoptosis pathway [7]. In pancreatic cancer, esculetin has been found to bind to KEAP1, inhibiting its interaction with Nrf2 and promoting the nuclear accumulation of Nrf2, which subsequently induces antiproliferative and apoptotic responses by attenuating NF-κB signaling [8]. In endometrial cancer, esculetin has been shown to exert anti-tumor effects by binding to hnRNPA1 and downregulating the transcription and translation of BCLXL and XIAP mRNA, thereby inducing apoptosis and arresting proliferation [9]. Furthermore, esculetin has been demonstrated to induce apoptosis and autophagy in leukemia cells and inhibit the Raf/MEK/ERK signaling pathway [10]. Additionally, recent findings have shown that esculetin induces apoptosis in ovarian cancer cells through the accumulation of excessive reactive oxygen species (ROS) and inhibition of the JAK2/STAT3 signaling pathway [11]. However, it is still unclear whether esculetin can induce other forms of cell death, such as ferroptosis, in tumor cells.

Ferroptosis is a novel form of programmed cell death characterized by intracellular iron accumulation and lipid peroxidation (LPO) [12]. Morphologically, ferroptotic cells can be distinguished by the presence of shrunken mitochondria with increased membrane density and reduced ridges [13]. The Fenton reaction

* Corresponding author.
E-mail addresses: lixianmei33@163.com (X. Li); zfh0606@fjmu.edu.cn (F. Zhang)

https://doi.org/10.1016/S1875-5364(25)60853-3

between fatty acids and iron ions in the cytoplasm generates lipid ROS. The Nrf2-xCT/GPx4 axis plays a central role in regulating ferroptosis. xCT facilitates the transport of cystine into the cytoplasm, where it serves as a raw material for the production of the antioxidant glutathione (GSH). GPX4 utilizes GSH to eliminate lipid ROS, thereby preventing cellular damage [14]. Nrf2 is a key transcription factor that controls the expression of both xCT and GPX4 [15]. Moreover, various proteins and genes, including ferritin heavy chain 1 (FTH1), achaete-scute family bHLH transcription factor 4 (ASCL4), and NADPH oxidase 1 (NOX1), contribute to the regulation of ferroptosis by controlling iron storage, polyunsaturated fatty acid (PUFA) metabolism, and redox balance, respectively [16-18]. Cancer cells often exhibit increased iron uptake, which can sensitize them to ferroptosis [19]. In recent years, inducing ferroptosis in tumor cells has emerged as a promising approach for cancer treatment. Several chemicals derived from traditional Chinese medicines (TCMs) have been found to exert anticancer effects by triggering ferroptosis [20-22]. However, whether esculetin can induce ferroptosis in HCC cells remains uncertain.

The zebrafish tumor xenograft model provides a novel alternative platform for investigating the anticancer properties of drugs *in vivo*. This model is cost-effective and time-saving, and the transparent zebrafish embryos enable direct assessment of tumor cell proliferation and metastasis using fluorescence imaging, which is advantageous compared to mouse models. This model has already demonstrated utility in elucidating the anti-HCC effects of natural compounds such as aloperine (ALO) and theabrownin (TB) [23, 24].

This study demonstrates that esculetin significantly inhibited the growth of HCC cells both *in vitro* and *in vivo*. Mechanistically, esculetin triggered ferroptosis by suppressing the Nrf2-xCT/GPx4 axis signaling pathway. These findings suggest the potential of esculetin as a therapeutic candidate for HCC treatment.

2. Materials and Methods

2.1. Cell culture

The human HCC cell lines Hep3B, Huh-7, and MHCC97H were obtained from the American Type Culture Collection (ATCC, USA). The cell lines were authenticated through short tandem repeat profiling. The cells were cultivated in Dulbecco's modified Eagle's medium (DMEM) (Boster, China) supplemented with 10% fetal bovine serum (FBS) (PAN, Germany) and 1% penicillin-streptomycin solution (HyClone, USA). The cells were cultured in a 5% CO_2 incubator at 37 °C.

2.2. Reagents and antibodies

Esculetin and ferrostatin-1 (Fer-1) were obtained from MedChemExpress (MCE, New Jersey, USA), and the compounds were dissolved in dimethylsulfoxide (DMSO) (Sigma, USA) and stored at −20 °C for subsequent use. Z-VAD-FMK and necrostatin-1 were purchased from Beyotime (Shanghai, China). The primary antibodies utilized in this study included ACTB (1∶2000) (Servebio, China), H3 (1∶1000) (Beyotime, China), NRF2 (1∶1000) (ABclonal, China), ACSL4 (1∶1000) (ABclonal, China), NOX1 (1∶500) (ABclonal, China), FHC (1∶1000) (ABclonal, China), GPX4 (1∶1000) (ABclonal, China), and SLC7A11 (1∶1000) (ABclonal, China).

2.3. Zebrafish husbandry and maintenance

The experiments involving animals were conducted in adherence to the Guide for the Care and Use of Laboratory Animals at Fujian Medical University.

The wild-type (WT) zebrafish line, obtained from the China Zebrafish Resource Center (Wuhan, China), was maintained at 28 °C with a 14 h/10 h light and dark cycle. Embryos were collected from natural fertilization, and the stages of embryonic development were determined according to established guidelines [25].

2.4. Cell viability assay

Cells were seeded into 96-well plates at a density of 4 000 cells per well. After 12 h, the experimental groups were treated with esculetin at concentrations of 28, 56, 112, 224, and 448 μmol·L^{-1}. The control group received 0.1% DMSO. Cell viability was assessed using a Cell Counting Kit-8 (CCK-8) (Servicebio, China) according to the manufacturer's protocol. *Cell viability* = 100% × *absorbance of (experimental group − blank control group)/absorbance of (control group − blank control group).* The half-maximal inhibitory concentration (IC_{50}) value was determined through non-linear regression analysis.

2.5. Cell death assay

Cell death was assessed by trypan blue exclusion assay. After treatment with varying concentrations of Esc (0−448 μmol·L^{-1}) at different time points, both suspended and adherent cells were collected and stained with 0.4% trypan blue dye for 3 min at room temperature. The stained cells were then counted using a hemocytometer under a light microscope.

2.6. Colony formation assay

Hep3B cells were seeded in 6-well plates at a density of 1,000 cells per well. The following day, the cells were treated with varying concentrations of esculetin (28, 56, and 112 μmol·L^{-1}) or 0.1% dimethylsulfoxide (DMSO) as a control. After 10 days, the cells were fixed with 4% paraformaldehyde (PFA) for 20 min and stained with crystal violet solution (Servicebio, China) for 10 min. The colony formation rate was calculated as (*number of colonies/cells seeded*) × 100%, and the results were normalized to the control group.

2.7. EdU proliferation assay

Cell proliferation was assessed using a Yefluro 594 EdU Imaging Kit (Yeasen, China) according to the manufacturer's protocol. Briefly, Hep3B cells were seeded into 48-well plates pre-fitted with coverslips. The cells were treated with varying concentrations of esculetin (28, 56, and 112 μmol·L^{-1}) or 0.1% DMSO as a control for 24 h post-adhesion. Cells were then incubated with 10 μmol·L^{-1} EdU for 2 h, fixed with 4% PFA for 15 min at room temperature, and washed with 3% BSA in phosphate-buffered saline (PBS). The remaining fixative was neutralized by incubating the cells with a 2 mg·mL^{-1} glycine solution for 5 min at room temperature. Subsequently, the cells were permeabilized with 0.5% Triton X-100 for 20 min. The cells were then incubated with Click-iT solution for 30 min at room temperature in the dark. Hoechst 33342 was used for nuclear staining. Finally, the coverslips were mounted on slides and observed under a TCS SP8 laser confocal scanning microscope (Leica, Germany). EdU-positive cells = *(Number of EdU − positive cells per field)/Number of all cells per field* × 100%.

2.8. Wound healing assay

HCC cells were seeded in a 6-well plate and cultured until they reached 90%−100% confluency. A uniform wound was created using the tip of a pipette. The detached cells and cellular debris were removed using PBS, and serum-free media contain-

ing varying concentrations of esculetin (28, 56, and 112 μmol·L^{-1}) or 0.1% dimethyl sulfoxide (DMSO) were added. After 24 h, images of the wound were captured using an inverted microscope for further analysis. The wound healing rate was calculated as follows: (*initial scratch width* − *final scratch width*)/*initial scratch width* × 100%. 112 μmol·L^{-1} or 0.1% DMSO were added. After 24 h, images of the wound were taken using an inverted microscope for additional analysis. Wound healing rate = (*initial scratch width* – *final scratch width*)/*initial scratch width* × 100%.

2.9. Transwell assay

Hep3B cells were pretreated with different concentrations of esculetin (28, 56, and 112 μmol·L^{-1}) or 0.1% DMSO as a control for 24 h. The cells were then trypsinized, diluted with serum-free medium, and seeded into the upper chamber at a density of 40 000 cells per well. The lower chamber contained medium supplemented with 20% FBS. After 48 h of incubation, the cells in the upper chamber were removed using a cotton swab. The invaded cells were then fixed with 4% PFA and stained with crystal violet. Images were captured under an inverted microscope at maximum magnification, and the number of invaded cells per field was quantified.

2.10. Cell apoptosis assay

Cell apoptosis was measured by employing a Fluorescein (FITC) TUNEL Cell Apoptosis Detection Kit (Servicebio, China) according to the manufacturer's instructions. The cell culture and drug treatment conditions were consistent with the EdU assay. Cells were washed with 1 × PBS, fixed with 4% PFA for 20 min, and then permeabilized with 0.5% Triton X-100 for 5 min. After a 10-minute incubation with equilibration buffer, the cells were incubated with TdT incubation buffer at 37 °C for 1 h in the dark. Cell nuclei were counterstained with DAPI (Biosharp, China). Finally, apoptotic cells were observed and photographed under a TCS SP8 laser confocal scanning microscope. TUNEL-positive cells = *Number of apoptotic cells per field/Number of all cells per field* × 100%.

2.11. Nuclei and cytoskeleton staining

Cells were treated with 112 μmol·L^{-1} esculetin or 0.1% DMSO for 24 h, then fixed in 4% PFA for 10 min. Following treatment with 0.1% Triton X-100 in PBS for 5 min, the cells were incubated in rhodamine-phalloidin staining solution (MesGen Biotech, China) at room temperature for 30 min. Cell nuclei were counterstained with DAPI. Finally, the cells were visualized and captured using a TCS SP8 laser confocal scanning microscope.

2.12. Ferrous ion (Fe^{2+}) detection

The intracellular Fe^{2+} levels were measured using a FerroOrange probe (Dojindo, Japan) according to the manufacturer's protocol. The cell culture and drug treatment procedures were consistent with the EdU assay. Following three washes with serum-free DMEM, the cells were incubated with a 1 μmol·L^{-1} FerroOrange working solution in a 5% CO_2 incubator at 37 °C for 30 min. The cells were then observed, and images were acquired using a TCS SP8 laser confocal scanning microscope.

To quantify the ferrous iron content, a Cell Ferrous Iron Colorimetric Assay Kit (Elabscience, China) was utilized. The ferrous iron content of HCC cells was determined following the manufacturer's instructions.

2.13. Detection of ROS

ROS levels were measured using a DCFH-DA fluorescence probe, following the manufacturer's instructions. Cells were cultured in a 24-well plate, and the drug treatment protocol aligned with the EdU assay. The cells were washed twice with 1× PBS and then incubated with a 10 μmol·L^{-1} DCFH-DA fluorescence probe at 37 °C for 1 h. Cell nuclei were counterstained with DAPI. Finally, the cells were observed and photographed under a Zeiss Axio Vert.A1 inverted fluorescence microscope (Zeiss, Germany).

2.14. Assessment of LPO

LPO was measured by employing Liperfluo (Dojindo, Japan) in accordance with the manufacturer's instructions. The cell culture and drug treatment procedures were consistent with the EdU assay. Cells were washed with serum-free Dulbecco's modified Eagle's medium (DMEM) and then incubated with a 5 μmol·L^{-1} Liperfluo working solution diluted with DMEM in an incubator at 37 °C for 30 min. Finally, the cells were observed and photographed under a Zeiss Axio Vert.A1 inverted fluorescence microscope.

2.15. Mitochondrial Membrane Potential Assessment

Mitochondrial membrane potential was evaluated using a JC-1 Mitochondrial Membrane Potential Assay Kit (Servicebio, China) according to the manufacturer's protocol. Cells were cultured in a 24-well plate, and the drug treatment regimen matched that of the EdU assay. Following drug exposure, the cells were washed twice with JC-1 dye buffer. Subsequently, equal volumes of serum-free DMEM and JC-1 staining solution were added, and the cells were incubated in a CO_2 incubator for 30 min in the dark. Finally, the cells were washed twice with JC-1 dye buffer and observed under a Zeiss Axio Vert.A1 inverted fluorescence microscope.

2.16. Determination of malondialdehyde (MDA), glutathione peroxidase (GSH-Px), GSH, hydrogen peroxide (H_2O_2), and catalase (CAT)

The biochemical indicators were determined using commercial kits, including the MDA assay kit (Servicebio, China), GSH-Px determination kit (Nanjing Jiancheng Bioengineering Institute, China), GSH assay kit (Beyotime, China), H_2O_2 Assay Kit (Beyotime, China), and CAT assay kit (Nanjing Jiancheng Bioengineering Institute, China), following the manufacturer's instructions.

2.17. Western blotting analysis

The cells were lysed with RIPA lysis buffer (Servicebio, China) and collected using a cell scraper. Nuclear protein was extracted using a commercial kit (Beyotime, China). The supernatant was collected after centrifugation, and the protein concentration was determined by a BCA Protein Assay Kit (Boster, China). Following denaturation at 98 °C, equal amounts of protein were separated by SDS-PAGE (Servicebio, China) and electrotransferred onto a PVDF membrane. The membrane was blocked in 5% fat-free milk for 1 hour at room temperature and then incubated with the primary antibodies overnight at 4 °C. After washing with 1 × TBST (Servicebio, China) three times, the membrane was incubated with secondary antibodies for 2–3 h at room temperature the following day. Finally, Amersham Image 600 (Cytiva, USA) was used to capture the exposure photos. ACTB or H3 was used as the internal control.

2.18. Immunofluorescence assay

Cells were initially fixed with 4% PFA in PBS. After thoroughly removing the PFA using PBS, non-specific antibody bind-

ing was blocked by incubating the cells in an ice-cold PBST solution containing bovine serum albumin (BSA) and DMSO (0.1% Triton-100, 1% BSA, and 1% DMSO in PBS, pH 7.4) for 1 h at room temperature. Subsequently, the cells were incubated overnight at 4 °C with a primary antibody against NRF2 (ABclonal, A21729) diluted in the blocking solution. Following this incubation, the cells were washed and then incubated overnight at 4 °C with a secondary antibody (anti-Rabbit IgG, Alexa Fluor 594) diluted at 1∶1000 in the blocking solution to detect the primary antibodies. After extensive washing, the cells were counterstained with DAPI to label the nuclei and then imaged using a TCS SP8 confocal microscope.

2.19. RNA extraction and RT-qPCR

Total RNA was extracted using the TRIZOL method. One microgram of RNA samples was reverse transcribed to generate first-strand cDNA utilizing the PrimeScriptTMRT Reagent Kit with the gDNA Eraser Kit (Takara, Beijing, China), and 1 μL of cDNA was employed for each reaction. RT-qPCR amplification was conducted using the iTaq™ Universal SYBR Green Supermix (Bio-Rad) on a CFX Connect Real-Time System (Bio-Rad, Wuhan, China). Actin served as the reference gene. The primers utilized are listed in Table S1, and fold-change values were calculated employing the $2^{-\Delta\Delta Ct}$ method.

2.20. Transmission electron microscopy

Following treatment with various chemicals, the cells were washed twice with 1× PBS, then digested with 0.25% trypsin and collected in a microtube. Subsequently, the cells were fixed in 2.5% glutaraldehyde for 1–2 h. The samples were then dehydrated, embedded, and cut into ultrathin sections (60–80 nm). After negative staining, the samples were observed under a transmission electron microscope (HT7800, HITACHI, Japan).

2.21. Cell transfection

The Nrf2 overexpression vector pCS2^{+}-Nrf2-SV40 was subcloned from the commercial plasmid pEnCMV-EGFP-2 × Linker-NFE2L2-SV40-Neo purchased from Miao Ling Biotechnology Co., Ltd. (Wuhan, China). Cells were seeded on 60 mm dishes and cultured until they reached 70%-80% confluence. Subsequently, the cells were transfected with 4 μg of the pCS2^{+}-Nrf2-SV40 plasmid or the pCS2^{+} empty vector as a negative control, using Lipofectamine 2000 reagent (Biosharp, China) according to the manufacturer's instructions. The transfected cells were then incubated with 112 μmol·L^{-1} esculetin or 0.1% DMSO for 24 h before harvesting.

2.22. Depletion of Nrf2 mRNA in Hep3B cells by shRNA interference

Lentiviral particles were produced through the cotransfection of VSVG, VPR, and pLKO.1 lentiviral vector containing the inserted Nrf2 shRNA sequences, as listed in Table S2. Viral-containing supernatants were harvested 48 h post-transfection. Exponentially growing cells were infected using the viral supernatant supplemented with 8 μg·mL^{-1} Polybrene. In the lentiviral shRNA experiments, transduced cells underwent continuous selection in the presence of 2 μg·mL^{-1} puromycin.

2.23. Zebrafish tumor xenograft assay

Hep3B cells were dissociated with 0.25% trypsin and washed with PBS three times. The cells were labeled with the red fluorescent cell tracker CM-DiI (Invitrogen, USA) according to the manufacturer's protocol. Approximately 500 or 300 labeled cells were then injected into the yolk sac or ventral perivitelline space of 48-hour post-fertilization (hpf) zebrafish larvae to establish a xenograft model for evaluating the proliferation or migration ability of HCC cells *in vivo*, respectively. At 2 h post-transplantation (hpt), embryos with comparable fluorescence areas in the yolk sac or ventral perivitelline space were selected for chemical treatment. Images were captured using a Nikon SMZ1270i stereo fluorescence microscope (Nikon, Japan) and analyzed with ImageJ software [26].

2.24. Statistical analysis

All experiments were conducted in triplicate. The data are presented as the mean ± standard error of the mean (SEM). Statistical comparisons between groups were performed using GraphPad Prism software version 8. Student's *t*-test and one-way analysis of variance (ANOVA) were utilized for statistical analysis. A P-value ≤ 0.05 was deemed statistically significant.

3. Results

3.1. Esculetin inhibits HCC proliferation, migration, and invasion

To investigate the anticancer effect of esculetin on HCC, three HCC cell lines, including Hep3B, MHCC97H, and Huh7, were utilized. CCK-8 assays demonstrated that esculetin significantly inhibited cell viability in all three HCC cell lines, with IC_{50} values of 74.87, 349.6, and 522.6 μmol·L^{-1} at 24 h for Hep3B, MHCC97H, and Huh7 cells, respectively (Figs. 1A–1C). Furthermore, the CCK-8 assay revealed that esculetin robustly inhibited the growth of Hep3B, MHCC97H, and Huh7 cells ($P < 0.05$), with the degree of inhibition increasing in a dose-dependent manner from 0 to 448 μmol·L^{-1} (Figs. 1D–1F) and in a time-dependent manner at 112 μmol·L^{-1} from 24 to 72 h (Figs. 1G–1I). To confirm the occurrence of cell death, a cell death assay by trypan blue staining was performed, and the results showed that esculetin also caused cell death of all three HCC cell lines in a dose and time-dependent manner (Fig. S1). Based on the IC_{50} values and the degree of inhibition, Hep3B cells were found to be more sensitive to esculetin compared to the other two HCC cell lines. Therefore, Hep3B cells were selected for further experiments, and esculetin concentrations of 28, 56, and 112 μmol·L^{-1} were chosen as low, medium, and high concentrations to test the dose-dependent effects.

As shown in Figs. 2A–2D, the colony formation and EdU assays revealed a significant, dose-dependent inhibition of Hep3B proliferation by esculetin at concentrations ranging from 0 to 112 μmol·L^{-1}. Additionally, the wound healing and Transwell assays demonstrated that esculetin significantly decreased the migration and invasion abilities of Hep3B cells compared to the control group (Figs. 2E–2H). Notably, a lower concentration (14 μmol·L^{-1}) of esculetin, which had no effect on cell viability, could still obviously reduce cell migration and invasion abilities, confirming that esculetin can specifically inhibit cell migration and invasion (Fig. S2).

3.2. Esculetin induces ferroptosis in Hep3B cells through inhibiting the Nrf2-xCT/GPx4 axis signaling

The potential pro-apoptotic effect of esculetin on Hep3B cells was assessed using a TUNEL assay. However, the results indicated that few apoptotic cells were observed, with or without exposure to esculetin (Figs. 3A and 3B). Interestingly, it was observed that Hep3B cells enlarged in size in a dose-dependent manner after treatment with esculetin (Figs. 3C and 3D). An ex-

amination of the ultrastructural characteristics of esculetin-treated Hep3B cells revealed that the cell membrane was not broken but rather blistered (Figs. 3E and 3F), a phenomenon consistent with some features of ferroptosis [27].

Ferroptosis is a form of programmed cell death characterized by iron overload and LPO [28]. To confirm the pro-ferroptosis effect of esculetin on Hep3B cells, the Fe^{2+} content was measured using FerroOrange staining and a cell ferrous iron colorimetric assay kit. FerroOrange staining revealed a dose-dependent increase in red fluorescence intensity, indicating elevated Fe^{2+} content in the esculetin-treated groups (Fig. 4A). Direct analysis of ferrous iron content further confirmed the accumulation of iron induced by esculetin in Hep3B cells (Fig. 4B). Excessive ferrous iron can trigger ferroptosis by promoting the accumulation of ROS and initiating Fenton reactions that mediate LPO [29]. The levels of LPO were detected using the Liperfluo probe, and esculetin was found to significantly promote LPO production in a dose-dependent manner (Figs. 4C and 4D).

Molecular investigation reveals that esculetin inhibits the activity of the Nrf2-xCT/GPx4 axis signaling pathway and modulates the expression of key regulators involved in ferroptosis. The xCT/GPx4 axis is a critical pathway regulating ferroptosis [29], and NRF2 plays a crucial role in controlling the expression of both xCT and GPX4 [15]. According to RT-qPCR results, 56 and 112 μmol·L^{-1} esculetin could downregulate the mRNA expression of *Nrf2* in Hep3B cells (Fig. S3). Western blotting analysis demonstrated that the protein levels of NRF2, SLC7A11 (xCT), and GPX4 were significantly reduced following esculetin treatment compared to the control group (Figs. 4E–4H). Additionally, the expression of FTH1, a subunit of ferritin responsible for iron storage [18], decreased upon esculetin exposure (Figs. 4I and 4J). Conversely, the expression levels of two pro-ferroptosis factors, ASCL4 and NOX1, which are involved in PUFA metabolism [17] and redox regulation [16], respectively, were significantly upregulated after esculetin treatment (Figs. 4I, 4K and 4L).

In conclusion, this study demonstrates that esculetin induces ferroptosis in HCC cells primarily by inhibiting the activity of the Nrf2-xCT/GPx4 axis signaling pathway.

3.3. Esculetin induces oxidative stress and mitochondrial damage in Hep3B cells

Ferroptosis and oxidative stress are intrinsically connected biological processes. The Fenton reaction, characterized by the interaction of iron with H_2O_2, plays a fundamental role in driving ferroptosis [30]. This reaction generates highly reactive hydroxyl radicals (•OH) that initiate LPO, leading to the production of harmful lipid peroxides that compromise cell membrane integrity [31].

To evaluate the level of oxidative stress in Hep3B cells fol-

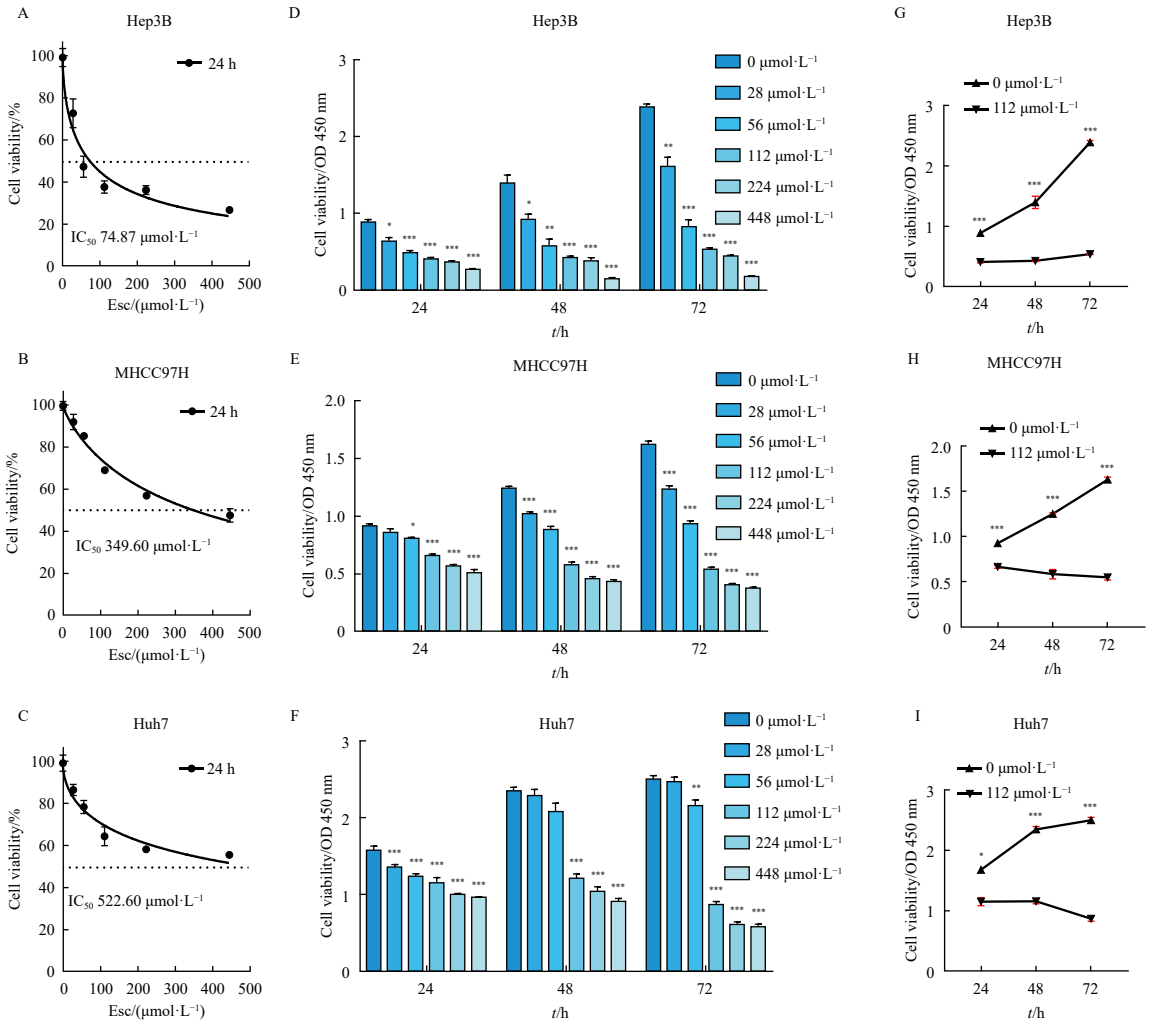

Fig. 1 Esculetin inhibits the viability of HCC cells in a dose- and time-dependent manner. (A–C) The IC_{50} of esculetin was determined in Hep3B, MHCC97H, and Huh7 cell lines after 24 h of treatment. (D–F) The cell viability of Hep3B, MHCC97H, and Huh7 cells was reduced by 0-448 μmol·L^{-1} esculetin. (G–I) The cell viability of Hep3B, MHCC97H, and Huh7 cells was inhibited by 112 μmol·L^{-1} esculetin over a period of 24 to 72 h. Each experiment was performed in triplicate (n = 3); the data are presented as mean ± standard error of the mean (SEM). Esc, esculetin; $^{*}P < 0.05$, $^{**}P < 0.01$, and $^{***}P < 0.001$ vs Control.

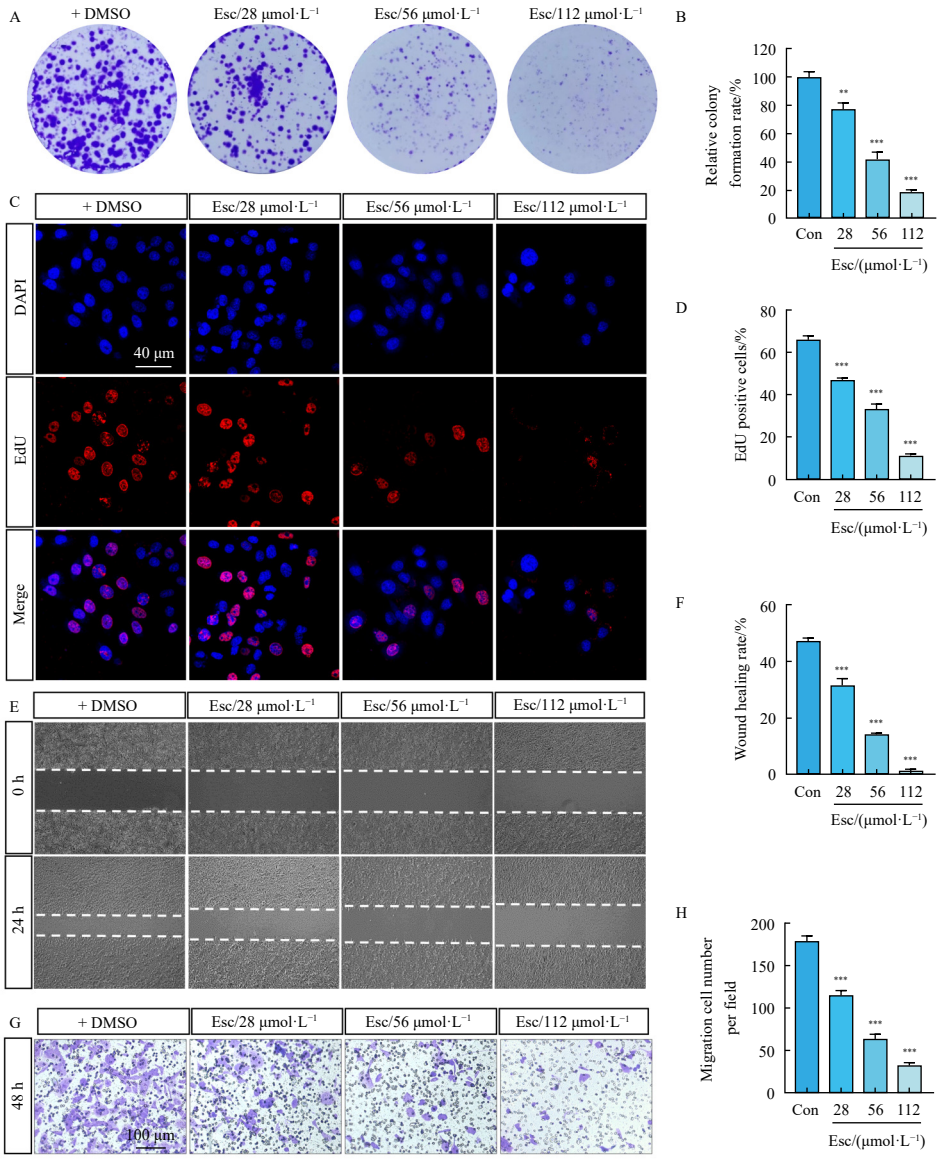

Fig. 2 Esculetin inhibits the proliferation, migration, and invasion of HCC cells in a dose-dependent manner. (A–B) Esculetin (0–112 μmol·L^{-1}) reduced the clonality of Hep3B cells in a dose-dependent manner, as quantified through analysis. (C–D) The EdU proliferation assay demonstrated that esculetin inhibited the proliferation of Hep3B cells in a dose-dependent manner, with the proliferation rates calculated. (E–F) The wound healing assay showed that esculetin inhibited the migration of Hep3B cells, with the results quantified. (G–H) Transwell assays revealed that esculetin impaired the invasion of Hep3B cells, with the quantitative analyses provided. Each experiment was replicated 3 times (n = 3), with the results presented as mean ± SEM. Con: control; Esc: esculetin; $^{**}P < 0.01$, $^{***}P < 0.001$ *vs* Con.

lowing esculetin treatment, several measurements were conducted. Firstly, the level of ROS was significantly elevated by esculetin at different concentrations, as demonstrated by DCFH-DA staining (Figs. 5A and 5B). MDA, a byproduct of LPO, was markedly increased by the administration of 56 and 112 μmol·L^{-1} esculetin for 24 h, indicating a higher degree of oxidative stress (Fig. 5C). Furthermore, the intracellular content of H_2O_2 was significantly increased (Fig. 5D), while the activity of GSH-Px and CAT was strongly inhibited by esculetin treatment in Hep3B cells (Figs. 5E and 5F). Moreover, GSH content was also significantly decreased when treated with 112 μmol·L^{-1} esculetin for 24 h (Fig. S4).

Furthermore, the study assessed mitochondrial membrane potential (MMP) as an indicator of mitochondrial function. The loss of MMP signifies mitochondrial dysfunction, which is associated with ferroptosis [32]. Typically, a healthy mitochondrial electrochemical potential gradient leads to the accumulation of the dye JC-1 in the mitochondrial matrix, forming red fluorescent aggregates. Conversely, a loss of MMP prevents this accumulation, resulting in a shift from red fluorescence (JC-1 aggregates) to green fluorescence (JC-1 monomers). The analysis revealed that esculetin-treated Hep3B cells exhibited a significantly higher proportion of JC-1 monomers compared to the DMSO-treated group, indicating a reduction in MMP (Figs. 5G and 5H).

The presented cytobiological and biochemical evidence indicates that esculetin induces oxidative stress and mitochondrial damage, ultimately resulting in ferroptotic cell death in Hep3B cells.

3.4. Fer-1 reverses the anti-tumor effect of esculetin in HCC cells

To confirm the involvement of ferroptosis in the anti-HCC activity of esculetin, the ferroptosis inhibitor Fer-1 was utilized to reverse the suppressive effect of esculetin on HCC cells. It was observed that Fer-1 significantly alleviated the cytotoxicity induced by esculetin (Fig. 6A). However, when both necroptosis and apoptosis inhibitors (necrostatin-1 and Z-VAD-FMK, respectively) were combined to test the resistance to cell death induced by esculetin, it was found that the inhibited cell viability induced by esculetin could not be rescued by either of the inhibitors, indicating that the effect of esculetin was not due to apoptosis or necrosis

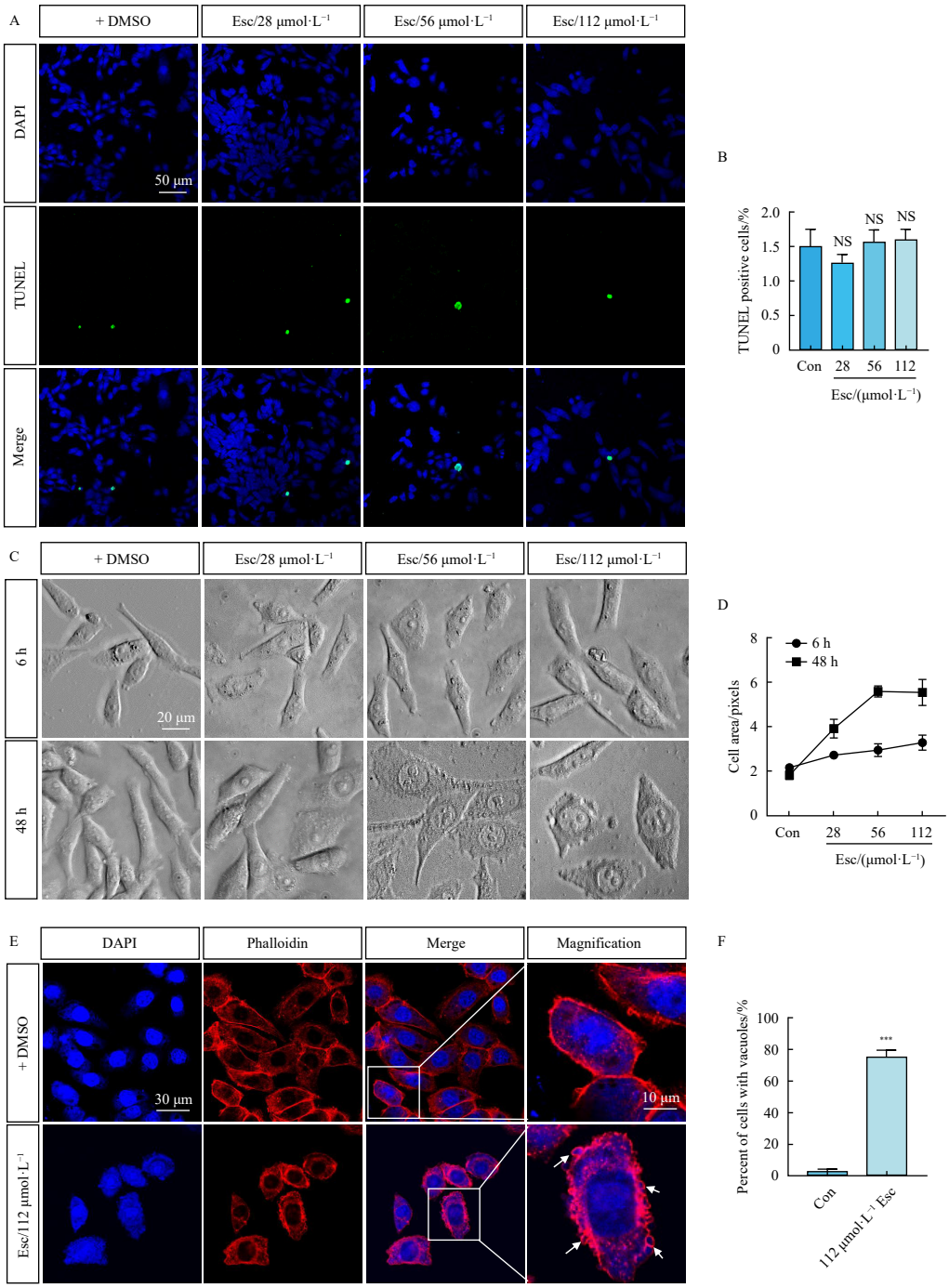

Fig. 3 Effects of esculetin on cell apoptosis and morphological changes in Hep3B cells. (A–B) A TUNEL assay kit was employed to detect apoptotic Hep3B cells after treatment with varying concentrations of esculetin (0–112 μmol·L^{-1}), and the quantification was examined. (C–D) The morphological changes in Hep3B cells were observed after exposure to esculetin (0–112 μmol·L^{-1}) for 6 or 48 h, and the statistics of cell area were analyzed. (E–F) Representative images of Hep3B cells co-stained with phalloidin and DAPI are shown after treatment with 112 μmol·L^{-1} esculetin or 0.1% DMSO for 24 h. The white arrows indicate the blistering of the cell membrane, and the number of cells with a blistered membrane was calculated. Each experiment was replicated 3 times (n = 3); mean ± SEM; Con: control; Esc: esculetin; NS: not significant; $^{***}P < 0.001$ vs Con.

(Fig. S5A). Moreover, the accumulation of intracellular Fe^{2+} induced by esculetin was significantly suppressed by Fer-1, as detected by FerroOrange staining and a commercial quantification kit (Figs. 6B and 6C).

Mitochondrial damage is a well-documented trigger of ferroptosis, a form of programmed cell death [33, 34]. To assess the association between esculetin and ferroptosis in HCC, we examined the morphological changes in mitochondria using transmission electron microscopy. The results showed that esculetin induced a decrease in mitochondrial volume and cristae, as well as an increase in membrane density in Hep3B cells compared to the DMSO-treated group (Fig. 6D, a and b). However, these disrupted mitochondrial morphology changes could be rescued by Fer-1, (Fig. 6D, b and d), indicating that esculetin-induced morphological changes in mitochondria were a consequence of ferroptosis. Furthermore, the accumulation of LPO (Figs. 6E and 6F) and ROS (Figs. 6G and 6H) induced by esculetin in Hep3B cells could be significantly decreased by Fer-1, as detected by Liperfluo and DCFH-DA staining, respectively. Fer-1 also significantly inhibited the upregulation of MDA content and restored the reduced GSH-Px activity as well as GSH content induced by esculetin in Hep3B cells (Figs. 6I and 6J, Fig. S4).

At the molecular level, the ferroptosis inhibitor Fer-1 partially reversed the downregulation of the NRF2, SLC7A11 (xCT),

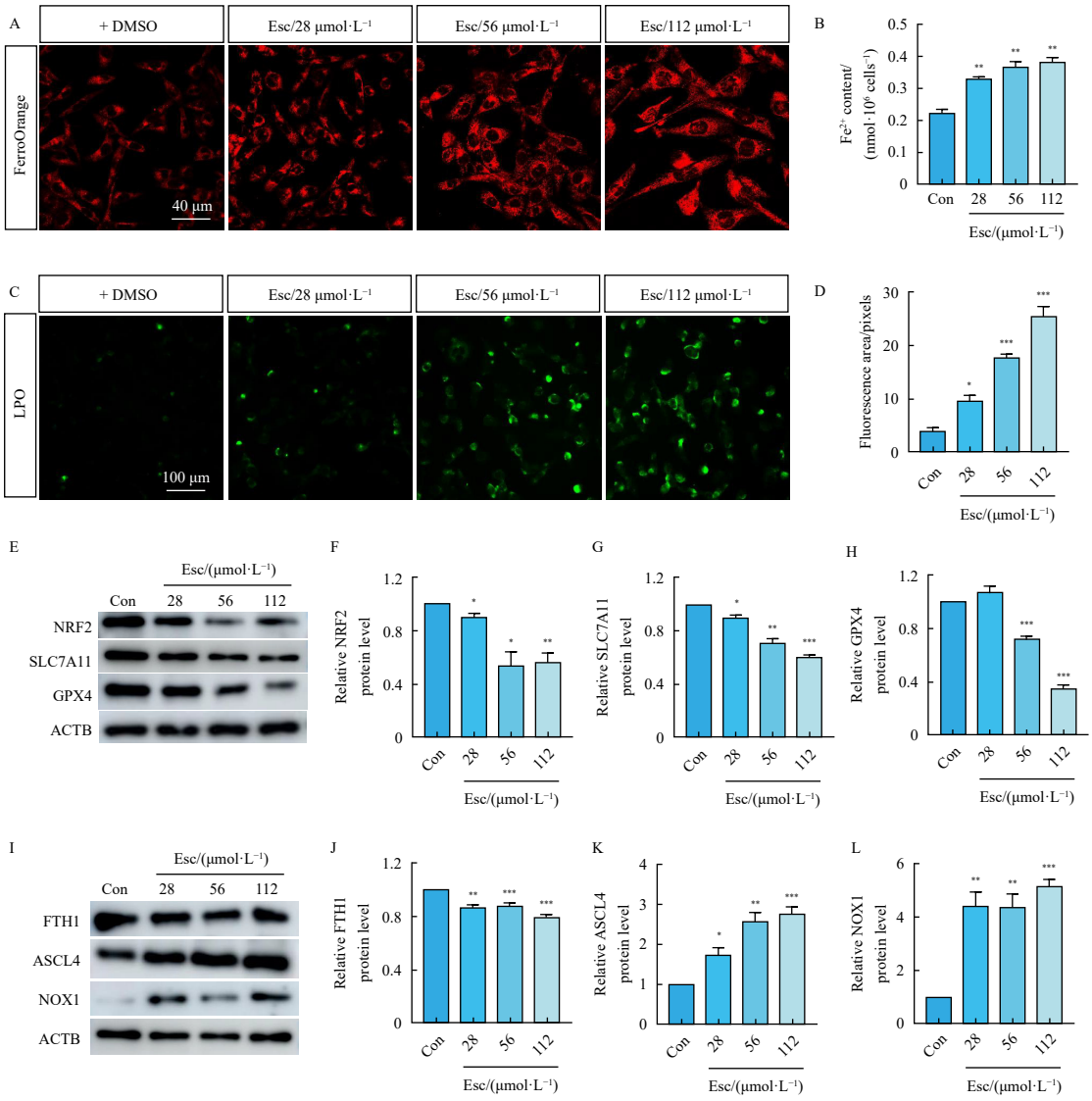

Fig. 4 Esculetin triggers ferroptosis in Hep3B cells *via* inhibition of the Nrf2-xCT/GPx4 axis signaling. (A) Fe^{2+} accumulation was examined using a Ferrorange probe in esculetin-treated Hep3B cells. (B) Intracellular ferrous ion content was determined using a commercial kit. (C–D) LPO of esculetin-treated Hep3B cells was detected by Liperfluo staining, and the fluorescence area was quantified. (E–H) The protein levels of NRF2, SLC7A11, and GPX4 in esculetin-treated Hep3B cells were examined by Western blotting and quantified. (I–L) The protein levels of FTH1, ASCL4, and NOX1 in esculetin-treated Hep3B cells were examined by Western blotting and quantified. Each experiment was replicated 3 times (n = 3); mean ± SEM; Con: control; Esc: esculetin; ACTB: actin beta; $^{*}P < 0.05$, $^{**}P < 0.01$, and $^{***}P < 0.001$ *vs* Con.

and GPX4 protein expression induced by esculetin (Figs. 6K–6N). However, co-treatment with both necroptosis and apoptosis inhibitors could not reverse the suppressed expression of these three proteins (Fig. S5B–S5E). Notably, immunofluorescence and Western blotting analyses revealed that esculetin significantly inhibited the translocation of the NRF2 protein into the nuclei of Hep3B cells, while Fer-1 prevented this inhibitory effect to some extent (Fig. S6).

To validate the capacity of esculetin to induce ferroptosis in additional HCC cell lines, we performed a series of experiments, including CCK-8 assays, GSH-Px and MDA detection, and FerroOrange, LPO, and ROS staining in both MHCC97H and Huh7 cells. Firstly, the ferroptosis inhibitor Fer-1 could attenuate the cytotoxicity induced by esculetin in both MHCC97H and Huh7 cells (Figs. S7A–S8A). Additionally, esculetin treatment resulted in a significant reduction in GSH-Px activity and an increase in MDA levels in these two cell lines, whereas Fer-1 co-treatment significantly increased GSH-Px activity and decreased MDA levels (Figs. S7B–S7C and S8B–S8C). Furthermore, esculetin exposure also led to the accumulation of intracellular Fe^{2+}, LPO, and ROS, but these effects were prevented by Fer-1 (Figs. S7D–S7I and S8D–S8I).

The findings presented indicate that the ferroptosis inhibitor Fer-1 can ameliorate the phenotypes associated with ferroptosis and reverse the anti-tumor effects of esculetin in HCC cells.

3.5. Nrf2 overexpression alleviates esculetin-induced ferroptosis in Hep3B cells

The results demonstrate that esculetin inhibits the Nrf2-xCT/GPx4 axis signaling activity in HCC cells. As Nrf2 plays a central role in this pathway, the study investigated whether overexpression of Nrf2 could potentially reverse the effects of esculetin-induced ferroptosis. As depicted in Figs. 7A–7D, the enforced overexpression of Nrf2 partially mitigated the downregulation of NRF2, SLC7A11, and GPX4 caused by esculetin treatment. Notably, Nrf2 overexpression also alleviated the substantial inhibition of cell viability induced by esculetin to some extent (Fig. 7E). Conversely, knockdown of Nrf2 by shRNA method significantly reduced the cell viability of Hep3B cells (Fig. S9). Additionally, the increased MDA content triggered by esculetin was downregulated upon Nrf2 overexpression (Fig. 7F), and the GSH-Px activity impaired by esculetin was significantly enhanced (Fig. 7G). Furthermore, overexpression of Nrf2 effectively constrained the accumulation of LPO induced by esculetin in HCC

cells (Figs. 7H and 7I). These findings collectively indicate that Nrf2 overexpression alleviates esculetin-induced ferroptosis in HCC cells, thereby highlighting the role of esculetin in triggering ferroptosis through the modulation of the Nrf2-xCT/GPx4 axis signaling.

3.6. Fer-1 partially reverses the anti-tumor effect of esculetin in a zebrafish xenograft model

To validate the anti-HCC effect of esculetin *in vivo*, a zebrafish tumor xenograft model was established to evaluate its ability to inhibit proliferation and metastasis in zebrafish embryos. Initially, the developmental toxicity of esculetin on zebrafish embryos was assessed by administering doses ranging from 0 to 1120 μmol·L^{-1} from 4 to 72 hpf. At 72 hpf, the embryos were classified into phenotypes: WT-like, C1 (mild malformations), C2 (moderate malformations), and C3 (severe malformations) (Fig. S10A). Statistical analysis revealed that treatment with 1120 μmol·L^{-1} esculetin resulted in approximately 43.3% C3, 46.3% C2, and 10.4% C1 phenotypes, while treatment with 560 μmol·L^{-1} esculetin led to approximately 3.3% C2, 85.6% C1, and 11.1% WT-like phenotypes. Concentrations ≤ 280 μmol·L^{-1} did not induce any defects (Fig. S10B). Additionally, only treatment with 1120 μmol·L^{-1} esculetin significantly reduced the hatching rate at 72 hpf and caused an approximate 4.4% death rate at 24 hpf (Figs. S10C and S10D).

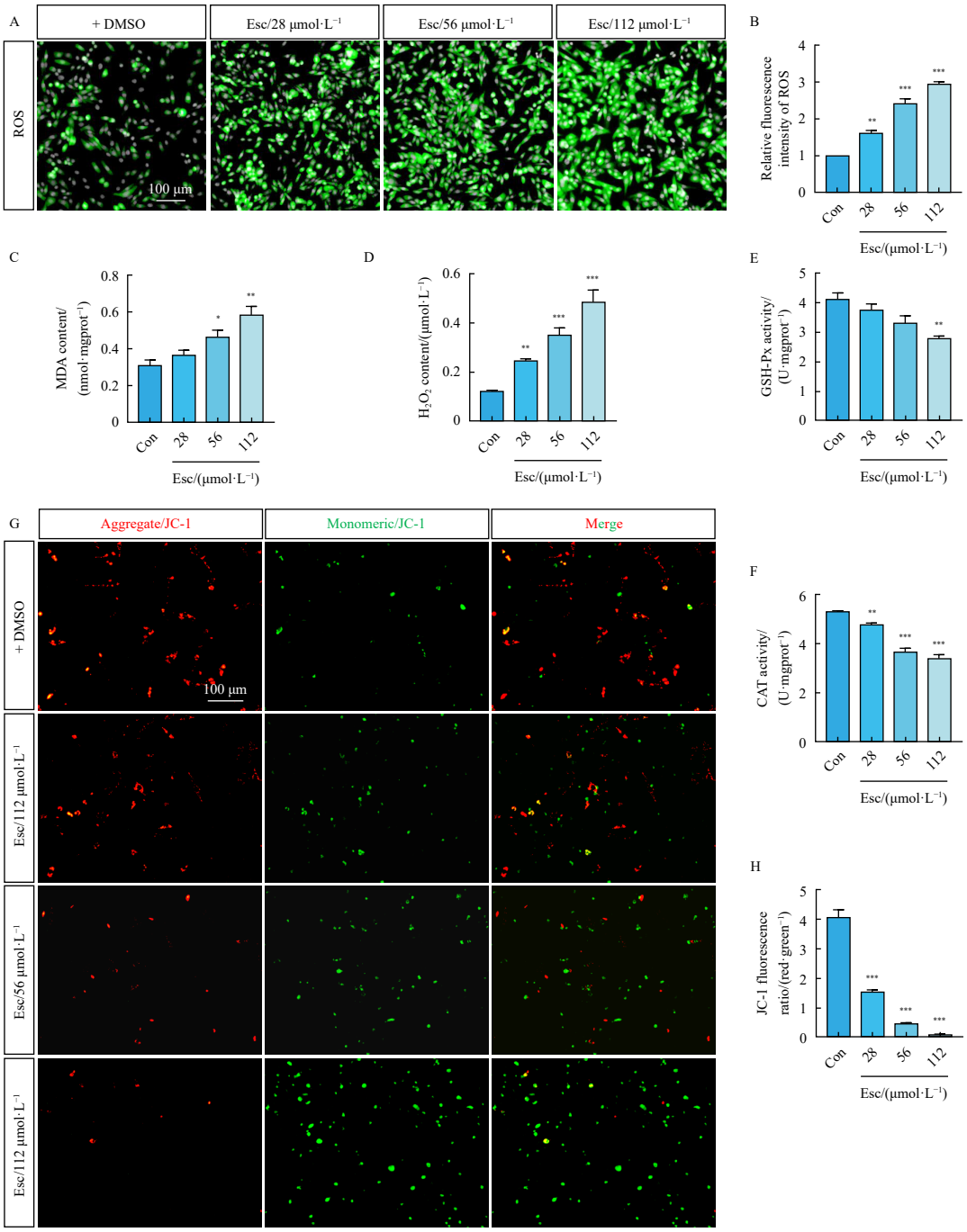

Fig. 5 Esculetin induces oxidative stress and mitochondrial damage in Hep3B cells. (A–B) The levels of ROS were detected through DCFH-DA staining in Hep3B cells treated with varying concentrations of esculetin. The fluorescence intensity was normalized to the DMSO-treated control group. (C–F) The contents of MDA, H_2O_2, and the activities of GSH-Px and CAT were examined in esculetin-treated Hep3B cells using commercial assay kits. The results for MDA, GSH-Px, and CAT were normalized to the corresponding total protein content. (G–H) Mitochondrial membrane potential was measured by JC-1 staining, and the ratio of red to green fluorescence was determined. Each experiment was replicated 3 times (n = 3); mean ± SEM; Con: control; Esc: esculetin; $^{*}P < 0.05$, $^{**}P < 0.01$, and $^{***}P < 0.001$ *vs* Con.

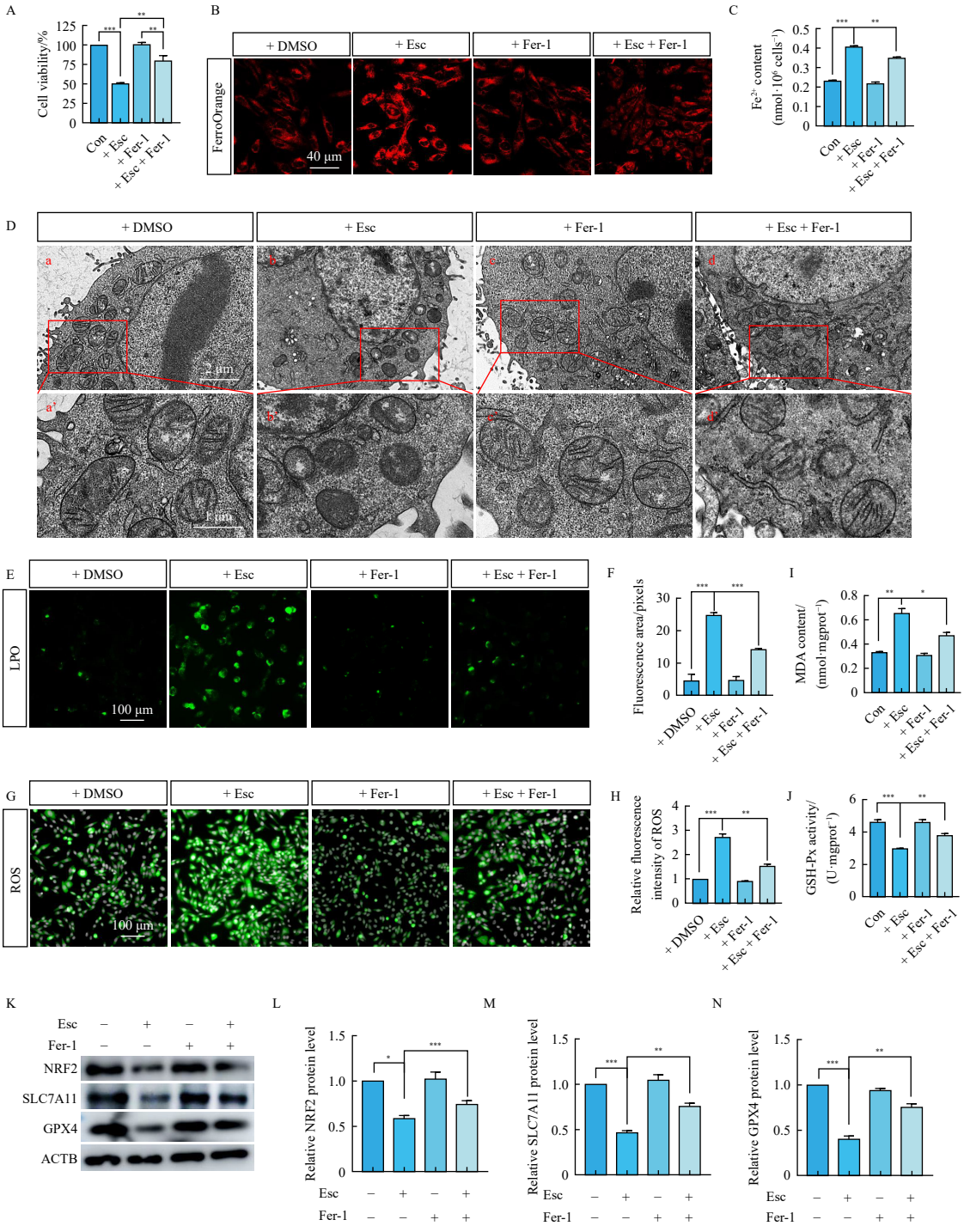

Fig. 6 Fer-1 reverses the anti-tumor effect of esculetin in HCC cells. (A) The cell viability of Hep3B cells was measured using the CCK-8 assay. (B) Fe^{2+} accumulation was examined in Hep3B cells treated with different chemicals, utilizing the FerroOrange probe. (C) The intracellular ferrous ion content was determined using a commercial kit. (D) Representative transmission electron microscopy images show the mitochondrial morphology, with a'–d' as magnifications of the images in the red boxes of a–d. (E–F) LPO in Hep3B cells treated with various chemicals was detected using Liperfluo staining, and the fluorescence area was quantified. (G–H) ROS levels in Hep3B cells treated with different chemicals were measured using DCFH-DA staining, and the fluorescence intensity was normalized to the DMSO-treated group. (I–J) The contents of MDA and GSH-Px were examined using commercial kits. (K–N) The qualitative and quantitative expression of NRF2, SLC7A11, and GPX4 in Hep3B cells treated with 112 μmol·L^{-1} esculetin and/or 1 μmol·L^{-1} Fer-1 for 24 h was evaluated by Western blotting. Each experiment was replicated 3 times (n = 3); mean ± SEM; Con: control; Esc: esculetin; ACTB: actin beta; $^{*}P < 0.05$, $^{**}P < 0.01$, and $^{***}P < 0.001$ *vs* Con.

Based on the developmental toxicity test results, we determined that 280 μmol·L^{-1} esculetin was a safe concentration and, therefore, administered it to the zebrafish xenografted embryos. To assess cell proliferation *in vivo*, approximately 500 Hep3B cells labeled with fluorescence were microinjected into the yolk sac of 2 days post-fertilization (dpf) WT zebrafish embryos. Esculetin and other chemicals were directly added to the culture media and incubated at 36 °C for 3 d. The proliferation of HCC cells could be evaluated by measuring changes in the fluorescence area. The results demonstrated that 280 μmol·L^{-1} esculetin effectively inhibited the proliferation of HCC cells in zebrafish embryos, while co-treatment with 10 μmol·L^{-1} Fer-1 partially reversed the inhibitory effect of esculetin *in vivo* (Figs. 8A and 8B). Similarly, we microinjected approximately 300 fluorescently labeled Hep3B cells into the ventral perivitelline space to assess cell migration in zebrafish embryos. The fluorescence area in the tail region was

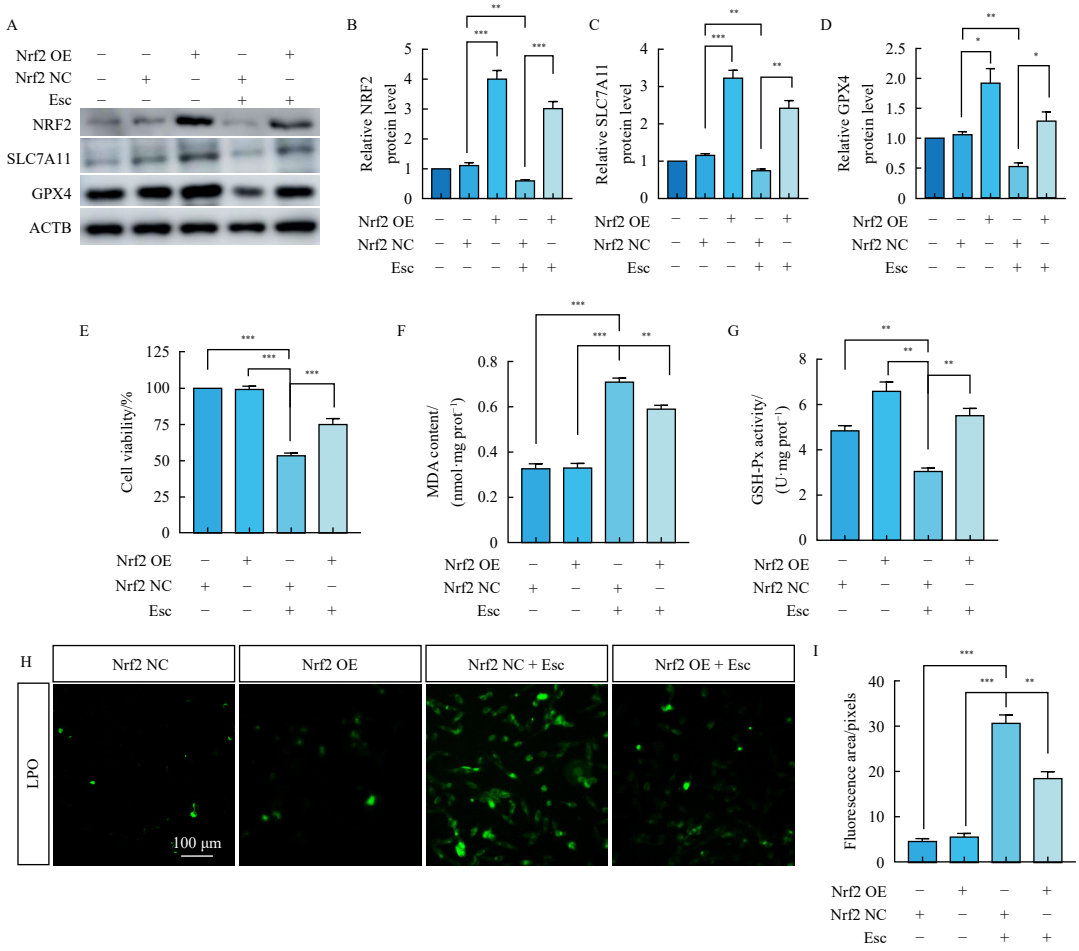

Fig. 7 Nrf2 overexpression alleviates esculetin-induced ferroptosis in Hep3B cells. (A–D) Western blotting analysis was conducted to examine the qualitative and quantitative expression of NRF2, SLC7A11, and GPX4 in esculetin-treated Nrf2 OE or NC Hep3B cells. (E) The cell viability of Hep3B cells in different groups was measured using the CCK-8 assay. (F–G) The contents of MDA and GSH-Px in the various groups were examined using commercial kits. (H–I) LPO in Hep3B cells across the different groups was detected by Liperfluo staining, and the fluorescence area was quantified. Each experiment was replicated 3 times (n = 3); mean ± SEM; OE: overexpression; NC: negative control; Esc: esculetin; ACTB: actin beta; $^{*}P < 0.05$, $^{**}P < 0.01$, and $^{***}P < 0.001$.

measured at 2 and 48 h post-transplantation (hpt). Esculetin at 280 μmol·L^{-1} also suppressed the migration of HCC cells to the tail region, while co-treatment with Fer-1 relieved this inhibition effect (Figs. 8C and 8D).

The findings collectively suggest that esculetin inhibits the proliferation and migration of HCC cells *in vivo* by inducing ferroptosis. Based on these results, we propose a mechanistic model to elucidate the underlying mechanism of the anti-HCC effect of esculetin (Fig. 9).

4. Discussion

HCC is the most prevalent form of liver cancer, and its incidence and mortality rates have been increasing annually [35]. The five-year survival rate for HCC is only around 30%–50%, and the rate of metastasis and recurrence within 5 years after surgery exceeds 60%, making it one of the most challenging prognoses among malignant tumors [36]. Consequently, there is an urgent need to develop new therapeutic drugs or approaches for HCC treatment. TCMs offer a unique resource for the development of frontline anti-tumor drugs. Several natural compounds derived from TCMs, such as ginsenoside and baicalin, have been found to exert anti-tumor effects against various cancer types, including HCC and OS [20, 37]. However, the underlying molecular mechanisms of these TCM-derived drugs in cancer treatment are still poorly understood. In the present study, we discovered that esculetin, a natural product found in the TCM Fraxini Cortex, could suppress HCC growth both *in vitro* and *in vivo* by inducing ferroptosis through the inhibition of the Nrf2-xCT/GPx4 axis signaling.

Previous research has documented that various natural compounds, including ALO, lappaconitine sulfate (LS), and TB, exert anti-HCC effects by inducing apoptosis [23, 24, 38]. Similarly, studies have shown that esculetin possesses anti-HCC properties by stimulating apoptosis in the SMMC-7721 HCC cell line [7, 39]. Additionally, esculetin has been found to induce apoptosis in other cancer cell types, such as human submandibular salivary gland tumor cells A253 [40], human endometrial cancer cells Ishikawa and HEC-1B [9], and human colorectal cancer cells HCT116, SW480, and HT-29 [41, 42]. However, in the current study, we observed that the cell death triggered by esculetin in the Hep3B HCC cell line was a result of ferroptosis rather than apoptosis. A recent study also demonstrated that esculetin can inhibit the growth of liver cancer cells (HUH7 and HCCLM3) by inducing ferritinophagy [43], which supported the findings of the present investigation. These studies collectively suggest that esculetin may induce either apoptosis or ferroptosis depending on the specific cancer cell lines being targeted.

Ferroptosis is characterized by iron overload and LPO resulting from oxidative stress. To investigate the ferroptotic phenotypes induced by esculetin in Hep3B cells, we measured intracellular Fe^{2+} content, ROS and LPO levels, as well as MDA and H_2O_2 content, and the activity of GSH-Px and CAT. As expected, the levels of pro-ferroptotic factors increased, while anti-ferroptotic factors decreased. Additionally, the well-characterized ferroptosis inhibitor Fer-1 partially reversed the phenotypes induced by esculetin, including decreased cell viability, MDA and iron accu-

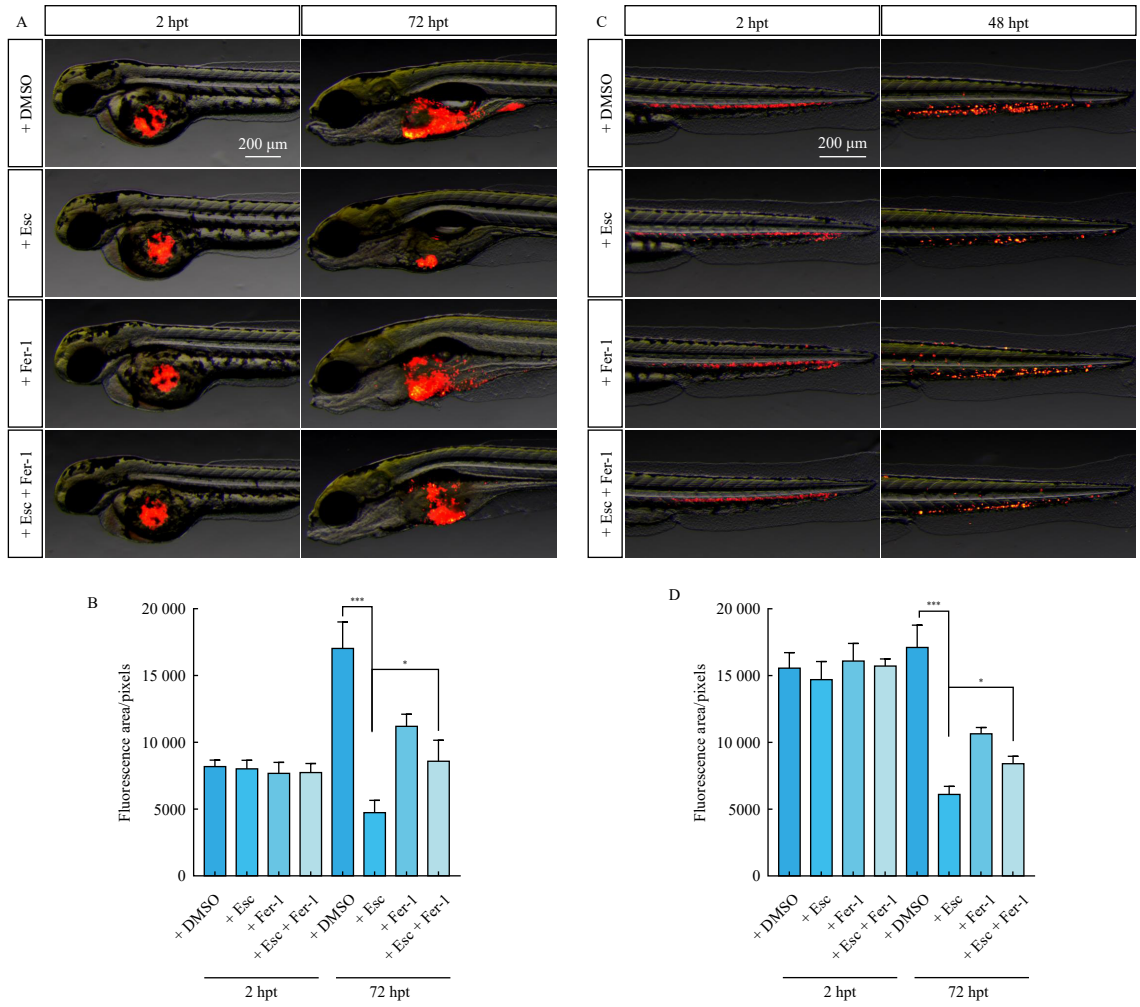

Fig. 8 Fer-1 partially reverses the anti-tumor effect of esculetin in a zebrafish xenograft model. (A–B) Representative images show the fluorescence area of tumor cells in zebrafish embryos treated with different chemicals, measured at 2 and 72 hpt. (C–D) Representative images illustrate the fluorescence area of metastatic tumor cells in the zebrafish tail region, measured at 2 and 48 hpt. Each experiment was replicated 3 times (n = 10); mean ± SEM. Esc: esculetin; hpt: h post-transplantation. $^{*}P < 0.05$, $^{***}P < 0.001$.

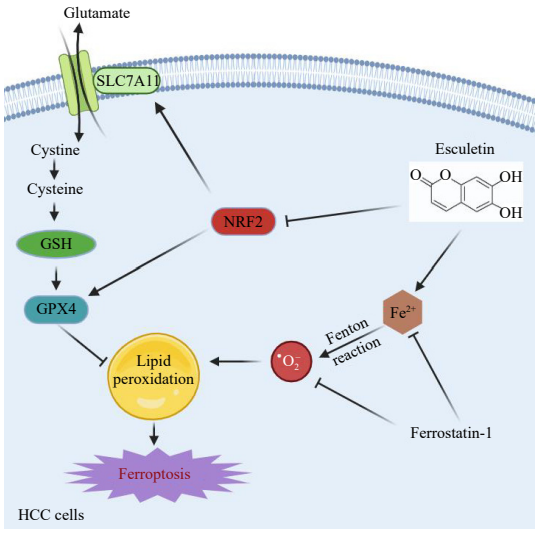

Fig. 9 A schematic diagram illustrating the underlying mechanism of esculetin-mediated anti-HCC activity.

mulation, loss of GSH-Px activity, and excessive ROS and LPO production. Morphological changes in mitochondria have also been identified as indicators of ferroptosis [44, 45]. We indeed observed morphological changes, including shrunken mitochondria, increased mitochondrial membrane density, and decreased mitochondrial cristae. Notably, Fer-1 reversed the disrupted mitochondrial morphology induced by esculetin. These findings provide confirmation that esculetin can induce ferroptosis in HCC cells. It is important to note that using another HCC cell line to verify these results would further strengthen the findings. Additionally, while the apoptosis and necrosis inhibitors Z-VAD-FMK and necrostatin-1 did not reverse the anti-HCC effect of esculetin, other forms of cell death, such as pyroptosis and autophagy, cannot be ruled out. Further experiments using targeted inhibitors specific to these types of cell death should be conducted to clarify the modes of cell death induced by esculetin.

The transcription factor Nrf2 plays a crucial role in antioxidant responses. Under oxidative stress, Nrf2 becomes activated and translocates into the nucleus, where it interacts with antioxidant response elements (AREs) to induce the expression of antioxidative genes [46]. Previous research has demonstrated that Nrf2 can protect against ferroptosis in HCC cells, and key proteins involved in ferroptosis, such as SLC7A11 and GPX4, are direct targets of Nrf2 [47, 48]. This study found that esculetin significantly suppressed the expression levels of NRF2, SLC7A11, and GPX4. However, treatment with the ferroptosis inhibitor Fer-1 prevented the esculetin-induced inhibition of NRF2, SLC7A11, and GPX4. Furthermore, overexpression of Nrf2 partially reversed the downregulation of SLC7A11 and GPX4 induced by esculetin and alleviated the ferroptosis phenotype. These findings suggest that esculetin induces ferroptosis in HCC cells by inhibiting the Nrf2-

xCT/GPx4 axis signaling. Nevertheless, it remains unclear whether esculetin directly regulates Nrf2. Some studies have shown that compounds like baicalin can directly interact with Nrf2 and affect its stability by inducing ubiquitin degradation, leading to ferroptosis in osteosarcoma cells [20]. In human endometrial cancer cells, esculetin can target hnRNPA1, thereby downregulating BCLXL and XIAP expression, resulting in apoptosis and cell proliferation arrest [9]. Therefore, it is important to explore the specific target protein of esculetin in HCC cells and elucidate the gene regulation network involved in its anti-tumor effects.

This study established a zebrafish tumor xenograft model to assess the anti-HCC effect of esculetin *in vivo*. The ferroptosis inhibitor Fer-1 partially reversed the anti-tumor effect of esculetin in zebrafish embryos, suggesting esculetin may inhibit HCC growth by inducing ferroptosis. Further elaborative experiments are required to conclusively confirm esculetin's ability to trigger ferroptosis and inhibit HCC growth in the zebrafish embryo model.

In summary, the findings of this study suggest that ferroptosis, a novel and significant mechanism, underlies the anti-HCC effects induced by esculetin. Esculetin triggers ferroptosis in HCC cells primarily through iron accumulation, mitochondrial disruption, and LPO. Inhibition of ferroptosis with the ferroptosis inhibitor Fer-1 or the enforced overexpression of the transcription factor nuclear factor erythroid 2-related factor 2 (Nrf2) effectively alleviates the ferroptosis outcome induced by esculetin, indicating that esculetin-triggered ferroptosis is caused by the inactivation of the Nrf2-xCT/glutathione peroxidase 4 (GPx4) axis signaling pathway. These findings may contribute to the development of esculetin as a potential therapeutic agent for the treatment of HCC.

5. Conclusion

The study demonstrated that esculetin, a natural compound derived from TCMs, possesses potent anti-HCC activity. Esculetin was found to induce ferroptosis, a form of regulated cell death characterized by iron overload and LPO, in HCC cells. This induction of ferroptosis was associated with the inhibition of the Nrf2-xCT/GPx4 axis signaling pathway. Esculetin treatment resulted in iron accumulation, disruption of mitochondrial morphology, increased levels of ROS and LPO products, as well as decreased activity of antioxidant enzymes. The ferroptosis inhibitor Fer-1 partially reversed the effects of esculetin, confirming its role in ferroptosis induction.

This study underscores the potential of esculetin as a therapeutic agent for the treatment of HCC. It elucidates the molecular mechanisms underlying esculetin's anti-HCC effects, identifying ferroptosis as a novel mechanism of action. These findings advance the understanding of the biological activities of esculetin and lay the groundwork for further research and development of esculetin-based therapies for HCC.

Funding

This work was supported by the Natural Science Foundations of Fujian Province (Nos. 2021J05063 and 2023J01541) and a startup grant for High-level Talents of Fujian Medical University (No. XRCZX2021014).

Supporting Information

Supporting data can be requested by sending E-mail to the corresponding authors.

Declaration of Competing Interest

These authors have no conflict of interest to declare

Acknowledgments

The authors gratefully thank Ling Lin from the Public Technology Service Center (Fujian Medical University, Fuzhou, China) for technical assistance.

References

1 Sung H, Ferlay J, Siegel RL, et al. Global Cancer Statistics 2020: GLOBOCAN estimates of incidence and mortality worldwide for 36 cancers in 185 countries. *CA Cancer J Clin*. 2021;71(3):209-249. https://doi.org/10.3322/caac.21660.
2 Villanueva A. Hepatocellular carcinoma. *N Engl J Med*. 2019;380(15):1450-1462. https://doi.org/10.1056/NEJMra1713263.
3 Vogel A, Qin S, Kudo M, et al. Lenvatinib versus sorafenib for first-line treatment of unresectable hepatocellular carcinoma: patient-reported outcomes from a randomised, open-label, non-inferiority, phase 3 trial. *Lancet Gastroenterol Hepatol*. 2021;6(8):649-658. https://doi.org/10.1016/S2468-1253(21)00110-2.
4 Jayakumar T, Huang CJ, Yen TL, et al. Activation of Nrf2 by esculetin mitigates inflammatory responses through suppression of NF-κB signaling cascade in RAW 264.7 Cells. *Molecules*. 2022;27(16):5143. https://doi.org/10.3390/molecules27165143.
5 Huang SX, Mou JF, Luo Q, et al. Anti-hepatitis B virus activity of esculetin from *Microsorium fortunei in vitro* and *in vivo*. *Molecules*. 2019;24(19):3475. https://doi.org/10.3390/molecules24193475.
6 Han MH, Park C, Lee DS, et al. Cytoprotective effects of esculetin against oxidative stress are associated with the upregulation of Nrf2-mediated NQO1 expression *via* the activation of the ERK pathway. *Int J Mol Med*. 2017;39(2):380-386. https://doi.org/10.3892/ijmm.2016.2834.
7 Wang J, Lu ML, Dai HL, et al. Esculetin, a coumarin derivative, exerts *in vitro* and *in vivo* antiproliferative activity against hepatocellular carcinoma by initiating a mitochondrial-dependent apoptosis pathway. *Braz J Med Biol Res*. 2015;48(3):245-253. https://doi.org/10.1590/1414-431x20144074.
8 Arora R, Sawney S, Saini V, et al. Esculetin induces antiproliferative and apoptotic response in pancreatic cancer cells by directly binding to KEAP1. *Mol Cancer*. 2016;15(1):64. https://doi.org/10.1186/s12943-016-0550-2.
9 Jiang R, Su G, Chen X, et al. Esculetin inhibits endometrial cancer proliferation and promotes apoptosis *via* hnRNPA1 to downregulate BCLXL and XIAP. *Cancer Lett*. 2021;521:308-321. https://doi.org/10.1016/j.canlet.2021.08.039.
10 Wang X, Yang C, Zhang Q, et al. *In vitro* anticancer effects of esculetin against human leukemia cell lines involves apoptotic cell death, autophagy, G_0/G_1 cell cycle arrest and modulation of Raf/MEK/ERK signalling pathway. *J BUON*. 2019;24(4):1686-1691.
11 Yin W, Fu X, Chang W, et al. Antiovarian cancer mechanism of esculetin: inducing G_0/G_1 arrest and apoptosis *via* JAK2/STAT3 signalling pathway. *J Pharm Pharmacol*. 2023;75(1):87-97. https://doi.org/10.1093/jpp/rgac083.
12 Dixon SJ, Lemberg KM, Lamprecht MR, et al. Ferroptosis: an iron-dependent form of nonapoptotic cell death. *Cell*. 2012;149(5):1060-1072. https://doi.org/10.1016/j.cell.2012.03.042.
13 Wu Y, Yu C, Luo M, et al. Ferroptosis in cancer treatment: another way to rome. *Front Oncol*. 2020;10:571127. https://doi.org/10.3389/fonc.2020.571127.
14 Carneiro BA, El-Deiry WS. Targeting apoptosis in cancer therapy. *Nat Rev Clin Oncol*. 2020;17(7):395-417. https://doi.org/10.1038/s41571-020-0341-y.
15 Dodson M, Castro-Portuguez R, Zhang DD. NRF2 plays a critical role in mitigating lipid peroxidation and ferroptosis. *Redox Biol*. 2019;23:101107. https://doi.org/10.1016/j.redox.2019.101107.
16 Leto TL, Morand S, Hurt D, et al. Targeting and regulation of reactive oxygen species generation by Nox family NADPH oxidases. *Antioxid Redox Signal*. 2009;11(10):2607-2619. https://doi.org/10.1089/ars.2009.2637.
17 Kuwata H, Hara S. Role of acyl-CoA synthetase ACSL4 in arachidonic acid metabolism. *Prostaglandins Other Lipid Mediat*. 2019;144:106363. https://doi.org/10.1016/j.prostaglandins.2019.106363.
18 Muhoberac BB, Vidal R. Iron, ferritin, hereditary ferritinopathy, and neurodegeneration. *Front Neurosci*. 2019;13:1195. https://doi.org/10.3389/fnins.2019.01195.
19 Chen MY, Juengpanich S, Hu JH, et al. Prognostic factors and predictors of postoperative adjuvant transcatheter arterial chemoembolization benefit in patients with resected hepatocellular carcinoma. *World J Gastroenterol*. 2020;26(10):1042-1055. https://doi.org/10.3748/wjg.v26.i10.1042.
20 Wen RJ, Dong X, Zhuang HW, et al. Baicalin induces ferroptosis in osteosarcomas through a novel Nrf2/xCT/GPX4 regulatory axis. *Phytomedicine*. 2023;116:154881. https://doi.org/10.1016/j.phymed.2023.154881.
21 Du X, Zhang J, Liu L, et al. A novel anticancer property of *Lycium barbarum* polysaccharide in triggering ferroptosis of breast cancer cells. *J Zhejiang Univ Sci B*. 2022;23(4):286-299. https://doi.org/10.1631/jzus.B2100748.
22 Li Q, Peng F, Yan X, et al. Inhibition of SLC7A11-GPX4 signal pathway is involved in aconitine-induced ferroptosis *in vivo* and *in vitro*. *J Ethnopharmacol*. 2023;303:116029. https://doi.org/10.1016/j.jep.2022.116029.
23 Liu JS, Huo CY, Cao HH, et al. Aloperine induces apoptosis and G_2/M cell cycle arrest in hepatocellular carcinoma cells through the PI3K/Akt signaling pathway. *Phytomedicine*. 2019;61:152843. https://doi.org/10.1016/j.phymed.2019.152843.
24 Xu J, Yan B, Zhang L, et al. Theabrownin induces apoptosis and tumor

inhibition of hepatocellular carcinoma Huh7 cells through ASK1-JNK-c-Jun pathway. *Onco Targets Ther*. 2020;13:8977-8987. https://doi.org/10.2147/OTT.S254693.
25 Kimmel CB, Ballard WW, Kimmel SR, et al. Stages of embryonic development of the zebrafish. *Dev Dyn*. 1995;203(3):253-310. https://doi.org/10.1002/aja.1002030302.
26 Schneider CA, Rasband WS, Eliceiri KW. NIH Image to ImageJ: 25 years of image analysis. *Nat Methods*. 2012;9(7):671-675. https://doi.org/10.1038/nmeth.2089.
27 Li F, Wang S, Zhou Y, et al. Signal transducer and activator of transcription 6 mediates skeletal muscle cell injury in septic mice by regulating ferroptosis. *Chin Crit Care Med*. 2023;35(8):813-817. https://doi.org/10.3760/cma.j.cn121430-20230312-00170.
28 Jiang X, Stockwell BR, Conrad M. Ferroptosis: mechanisms, biology and role in disease. *Nat Rev Mol Cell Biol*. 2021;22(4):266-282. https://doi.org/10.1038/s41580-020-00324-8.
29 Xing G, Meng L, Cao S, et al. PPARα alleviates iron overload-induced ferroptosis in mouse liver. *EMBO Rep*. 2022;23(8):e52280. https://doi.org/10.15252/embr.202052280.
30 Kobayashi H, Yoshimoto C, Matsubara S, et al. A comprehensive overview of recent developments on the mechanisms and pathways of ferroptosis in cancer: the potential implications for therapeutic strategies in ovarian cancer. *Cancer Drug Resist*. 2023;6(3):547-566. https://doi.org/10.20517/cdr.2023.49.
31 Conrad M, Pratt DA. The chemical basis of ferroptosis. *Nat Chem Biol*. 2019;15(12):1137-1147. https://doi.org/10.1038/s41589-019-0408-1.
32 Kuang F, Liu J, Tang D, et al. Oxidative damage and antioxidant defense in ferroptosis. *Front Cell Dev Biol*. 2020;8:586578. https://doi.org/10.3389/fcell.2020.586578.
33 Battaglia AM, Chirillo R, Aversa I, et al. Ferroptosis and cancer: mitochondria meet the "iron maiden" cell death. *Cells*. 2020;9(6):1505. https://doi.org/10.3390/cells9061505.
34 Jelinek A, Heyder L, Daude M, et al. Mitochondrial rescue prevents glutathione peroxidase-dependent ferroptosis. *Free Radic Biol Med*. 2018;117:45-57. https://doi.org/10.1016/j.freeradbiomed.2018.01.019.
35 Rumgay H, Arnold M, Ferlay J, et al. Global burden of primary liver cancer in 2020 and predictions to 2040. *J Hepatol*. 2022;77(6):1598-1606. https://doi.org/10.1016/j.jhep.2022.08.021.
36 Fan J, Tian L, Huang S, et al. Derlin-1 promotes the progression of human hepatocellular carcinoma *via* the activation of AKT pathway. *Onco Targets Ther*. 2020;13:5407-5417. https://doi.org/10.2147/OTT.S222895.
37 Tan X, Ma X, Dai Y, et al. A large-scale transcriptional analysis reveals herb-derived ginsenoside F2 suppressing hepatocellular carcinoma *via* inhibiting STAT3. *Phytomedicine*. 2023;120:155031. https://doi.org/10.1016/j.phymed.2023.155031.
38 Zhang X, Ma J, Song N, et al. Lappaconitine sulfate inhibits proliferation and induces apoptosis in human hepatocellular carcinoma HepG2 cells through the reactive oxygen species-dependent mitochondrial pathway. *Pharmacology*. 2020;105(11-12):705-714. https://doi.org/10.1159/000506081.
39 Li J, Li S, Wang X, et al. Esculetin induces apoptosis of SMMC-7721 cells through IGF-1/PI3K/Akt-mediated mitochondrial pathways. *Can J Physiol Pharmacol*. 2017;95(7):787-794. https://doi.org/10.1139/cjpp-2016-0548.
40 Park SB, Jung WK, Kim HR, et al. Esculetin has therapeutic potential *via* the proapoptotic signaling pathway in A253 human submandibular salivary gland tumor cells. *Exp Ther Med*. 2022;24(2):533. https://doi.org/10.3892/etm.2022.11460.
41 Kim WK, Byun WS, Chung HJ, et al. Esculetin suppresses tumor growth and metastasis by targeting Axin2/*E*-cadherin axis in colorectal cancer. *Biochem Pharmacol*. 2018;152:71-83. https://doi.org/10.1016/j.bcp.2018.03.009.
42 Kim AD, Madduma Hewage SR, Piao MJ, et al. Esculetin induces apoptosis in human colon cancer cells by inducing endoplasmic reticulum stress. *Cell Biochem Funct*. 2015;33(7):487-494. https://doi.org/10.1002/cbf.3146.
43 Xiu Z, Li Y, Fang J, et al. Inhibitory effects of esculetin on liver cancer through triggering NCOA4 pathway-mediation ferritinophagy *in vivo* and *in vitro*. *J Hepatocell Carcino*. 2023;10:611-629. https://doi.org/10.2147/JHC.S395617.
44 Xie Y, Hou W, Song X, et al. Ferroptosis: process and function. *Cell Death Differ*. 2016;23(3):369-379. https://doi.org/10.1038/cdd.2015.158.
45 Stockwell BR, Friedmann Angeli JP, Bayir H, et al. Ferroptosis: a regulated cell death nexus linking metabolism, redox biology, and disease. *Cell*. 2017;171(2):273-285. https://doi.org/10.1016/j.cell.2017.09.021.
46 Pan JA, Sun Y, Jiang YP, et al. TRIM21 ubiquitylates SQSTM1/p62 and suppresses protein sequestration to regulate redox homeostasis. *Mol Cell*. 2016;61(5):720-733. https://doi.org/10.1016/j.molcel.2016.02.007.
47 Lovatt M, Kocaba V, Hui Neo DJ, et al. Nrf2: a unifying transcription factor in the pathogenesis of Fuchs' endothelial corneal dystrophy. *Redox Biol*. 2020;37:101763. https://doi.org/10.1016/j.redox.2020.101763.
48 Yang WS, Stockwell BR. Ferroptosis: death by lipid peroxidation. *Trends Cell Biol*. 2016;26(3):165-176. https://doi.org/10.1016/j.tcb.2015.10.014.